Metal Ion-Induced Stabilization and Refolding of Anticoagulation Factor II from the Venom of *Agkistrodon acutus*†

Xiaolong Xu, Qingliang Liu,* and Yongshu Xie

Department of Chemistry, University of Science and Technology of China, Hefei 230026, Peoples Republic of China

Received October 1, 2001; Revised Manuscript Received December 30, 2001

ABSTRACT: Anticoagulation factor II (ACF II) isolated from the venom of *Agkistrodon acutus* is an activated coagulation factor X-binding protein in a Ca^{2+}-dependent fashion with marked anticoagulant activity. The equilibrium unfolding/refolding of apo-ACF II, holo-ACF II, and Tb^{3+}-reconstituted ACF II in guanidine hydrochloride (GdnHCl) solutions was studied by following the fluorescence and circular dichroism (CD). Metal ions were found to increase the structural stability of ACF II against GdnHCl and irreversible thermal denaturation and, furthermore, influence its unfolding/refolding behavior. The GdnHCl-induced unfolding/refolding of both apo-ACF II and Tb^{3+}-ACF II is a two-state process with no detectable intermediate state, while the GdnHCl-induced unfolding/refolding of holo-ACF II in the presence of 1 mM Ca^{2+} follows a three-state transition with an intermediate state. Ca^{2+} ions play an important role in the stabilization of both native and I states of holo-ACF II. The decalcification of holo-ACF II shifts the ending zone of unfolding/refolding curve toward lower GdnHCl concentration, while the reconstitution of apo-ACF II with Tb^{3+} ions shifts the initial zone of the denaturation curve toward higher GdnHCl concentration. Therefore, it is possible to find a denaturant concentration (2.1 M GdnHCl) at which refolding from the fully denatured state of apo-ACF II to the I state of holo-ACF II or to the native state of Tb^{3+}-ACF II can be initiated merely by adding the 1 mM Ca^{2+} ions or 10 μM Tb^{3+} ions to the unfolded state of apo-ACF II, respectively, without changing the concentration of the denaturant. Using Tb^{3+} as a fluorescence probe of Ca^{2+}, the kinetic results of metal ion-induced refolding provide evidence for the fact that the first phase of Tb^{3+}-induced refolding should involve the formation of the compact metal-binding site regions, and subsequently, the protein undergoes further conformational rearrangements to form the native structure.

Anticoagulation factor II (ACF II)[1] is a nonenzymatic anticoagulant from the venom of *Agkistrodon acutus* which has marked anticoagulant activity with a unique anticoagulant mechanism, for it forms a 1:1 complex with activated coagulation factor X (FXa) in a Ca^{2+}-dependent fashion and thereby blocks the amplification of the coagulation cascade (*1*, *2*). ACF II is a member of coagulation factor IX/coagulation factor X-binding protein family. The proteins of this family have very similar amino acid compositions and high homologous sequences and form 1:1 complexes with coagulation factor IX/activated coagulation factor IX or coagulation factor X/activated coagulation factor X and prolong the clotting time (*3*−*6*). All bindings are dependent on Ca^{2+} ions. In this family, the crystal structures of coagulation factor IX/factor X-binding protein (habu IX/X-bp) (*7*) and coagulation factor IX-binding protein (habu IX-bp) (*8*) purified from the habu snake have been reported. The ribbon model of habu IX/X-bp is shown in Figure 1

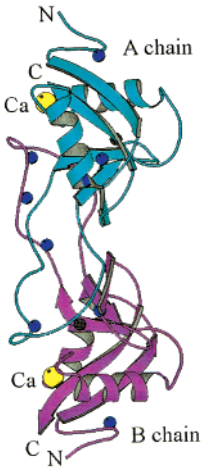

FIGURE 1: Ribbon model of the heterodimer polypeptide chains of habu IX/X-bp. The Ca^{2+} ions and Trp residues are indicated as large balls and small balls, respectively. The picture was drawn with Protein Data Bank file 1lXX (*7*).

(*7*). Both structures of habu IX/X-bp and habu IX-bp are almost identical with the same size of 7 nm × 3 nm × 3 nm. Each is a heterodimer protein consisting two homologous chains with a similar topology structure linked with a disulfide bond. Each chain has one Ca^{2+}-binding site. One of them is formed by Ser 41, Glu 43, Glu 47, and Glu 128 in the A chain, and the other site is formed by Ser 41, Gln

† The work is supported by grants from the National Natural Science Foundation of China (Grant 20171041 to X.X.) and the Natural Science Foundation of Anhui Province of China (Grant 00044428 to X.X.).

* To whom correspondence should be addressed. Tel: +86-551-3603214. Fax: +86-551-3603388. E-mail: qliu@ustc.edu.cn.

[1] Abbreviations: ACF II, anticoagulation factor II; FX, coagulation factor X; FXa, activated coagulation factor X; CD, circular dichroism; GdnHCl, guanidine hydrochloride; habu IX/X-bp, habu coagulation factor IX/factor X-binding protein; habu IX-bp, coagulation factor IX-binding protein; PPT, plasma prothrombin time.

10.1021/bi015819j CCC: $22.00
Published on Web 02/20/2002

43, Glu 47, and Glu 120 in the B chain, in habu IX/X-bp as well as in habu IX-bp.

ACF II consists of two chains with N-terminal amino acid sequences similar to those of habu IX/X-bp (unpublished data), and both proteins have a similar amino acid composition (*1*). ACF II has two Ca^{2+}-binding sites with different association constant values, $(1.1 \pm 0.3) \times 10^5\ M^{-1}$ and $(1.7 \pm 0.4) \times 10^4\ M^{-1}$ respectively (*2*), which are similar to that of habu IX/X-bp, respectively. Recently, the size of ACF II was determined to be 7.2 nm × 3.3 nm × 3.1 nm by atomic force microscopy (unpublished data), within experimental errors, which is similar to the sizes of habu IX/X-bp and habu IX-bp. In addition, ACF II has a secondary structure similar to that of habu IX/X-bp (see Results). It therefore is reasonable to assume that the fold does not differ much between ACF II and habu IX/X-bp or habu IX-bp. Thus, ACF II should contain α-helix and β-sheet conformations with similar structures of Ca^{2+}-binding sites to habu IX/X-bp and habu IX-bp.

ACF II is devoid of hemorrhagic and lethal activities, which may be useful both as a basis for designing anticoagulant drugs and as a convenient tool in exploration of the complex mechanisms of the coagulation cascade. The binding of ACF II to FXa is dependent on the concentration of Ca^{2+} ions, and the maximal binding of ACF II to FXa requires a concentration of Ca^{2+} ions of 1 mM. We expected that analysis of the effect of Ca^{2+} ions on the structural stability of ACF II would be useful for improving our understanding of the function of Ca^{2+} ions in the binding of ACF II to FXa. To examine the role of Ca^{2+} ions in the conformational stabilization of ACF II, studies on guanidine hydrochloride-(GdnHCl-) and thermal-induced denaturation and metal ion-induced refolding of ACF II were carried out in this paper. Tb^{3+}, as a fluorescence probe, has been widely used to study protein structural characteristics and therefore is expected to be used as a fluorescence probe of Ca^{2+} to monitor the mechanism of the unfolding/refolding of ACF II.

Protein folding/unfolding is a highly cooperative process. It has recently been demonstrated that the folding/unfolding of small globular proteins occurs via a two-state process, while the folding/unfolding of larger proteins (>100 amino acids) is complex and often involves the formation of intermediate(s) (*9*−*11*). Protein folding/unfolding can be affected by factors such as pressure (*12*−*14*), temperature (*15*−*18*), pH (*19*−*23*), and disulfide bond (*24*−*26*). Recently, the effects of metal ions and anions on protein unfolding/refolding have received considerable attention. It has been demonstrated that metal ion-induced conformation changes in several enzymes lead to stabilization of the proteins during protein folding/unfolding (*27*−*31*). In addition, without changing the concentration of the denaturant, the refolding of several proteins can be induced simply by adding anions (*32*, *33*) or cations (*34*).

The present investigation supports the fact that metal ions not only significantly increase the structural stability of ACF II against GdnHCl and thermal denaturation but also induce the refolding of the unfolded apo-ACF II merely by adding 1 mM Ca^{2+} or 10 μM Tb^{3+} to the unfolded apo-ACF II without changing the concentration of the denaturant, and furthermore, metal ions can influence the unfolding/refolding behavior of ACF II. Using Tb^{3+} as a fluorescence probe of Ca^{2+}, the metal ion-induced refolding kinetic studies suggest that the first phase of Tb^{3+}-induced refolding should involve the formation of the compact metal-binding site regions.

MATERIALS AND METHODS

Chemicals. Lyophilized venom powder was provided by the TUN-XI Snakebite Institute (Anhui, P. R. China). Guanidine hydrochloride (GdnHCl, ultrapure) and Tb_4O_7 (99.9%) were obtained from Sigma Chemical Co. (St. Louis, MO). Chelex-100 was purchased from Bio-Rad Laboratories (Richmond, CA). Rabbit brain thromboplastin was made by the Institute of Hematology, Chinese Academy of Medical Sciences (Tianjin, P. R. China). All other reagents were of analytical reagent grade. Milli-Q purified water was used throughout.

Protein Purification and Preparation. ACF II was purified by the method described previously (*1*). The apo-ACF II was prepared by dialysis of purified ACF II against a suspension of Chelex-100 (Bio-Rad) (1 g/L) in 0.01 M Tris-HCl (pH 8.0). ACF II concentration was calculated from the absorption coefficient ($A_{1cm}^{1\%} = 30$) at 280 nm and the relative molecular weight ($M_r = 29468$). Tb_4O_7 was dissolved in concentrated HCl by gentle heating to dryness and then dissolved in Milli-Q superpure water, and the pH value was adjusted to 6.0 with HCl or NaOH. The solution of Ca^{2+} ions was prepared from $CaCl_2$ in Milli-Q water. The solutions of Tb^{3+} and Ca^{2+} were standardized by titration with standard EDTA solution. Tris-HCl buffer used was freed from any possible contamination of multivalent cations by passage through a column (25 × 3 cm) of Chelex-100. GdnHCl was determined to be metal-free by extraction with dithizone (6 mg/L) in carbon tetrachloride. All utensils used during the experiments were made metal-free by soaking in 2 M HNO_3 for 24 h and then by extensively rinsing with Milli-Q purified water.

Steady-State Fluorescence Measurements. All fluorescence measurements were performed on a Shimadzu RF-5000 spectrofluorometer using a 10 mm quartz cuvette. The sample temperature was kept at 25.0 °C with a circulating water bath. In all experiments, the samples were excited at 295 nm, and the bandwidths for excitation and emission were both set to 5 nm. Each spectrum is the average of three consecutively acquired spectra. All spectra were corrected by subtracting the spectrum of the blank, lacking the protein but otherwise identical to the sample.

Circular Dichroism (CD) Measurements. CD measurements were carried out with a Jasco J-720 spectropolarimeter. The instrument was calibrated with *d*-10-camphorsulfonic acid. All of the CD measurements were made at 25 °C with a thermostatically controlled cell holder. Far-UV CD spectra were collected between 200 and 250 nm with a scan speed of 20 nm/min and a response time of 1 s, at a protein concentration of 0.10 mg/mL, in quartz cells of 1 mm path length. The obtained values were normalized by subtracting the baseline recorded for the buffer having the same concentration of salts under similar conditions. The data were expressed in mean residue ellipticity $[\theta]$ in deg·cm^2·dmol^{-1}, which is defined as $[\theta] = 100\theta_{obs}(lc)^{-1}$, where θ_{obs} is the observed ellipticity in degrees, c is the concentration in residue moles per liter, and l is the length of the light path in centimeters.

Denaturation and Renaturation Experiments. Solutions for the denaturation and renaturation experiments were prepared

from stock solutions of protein and GdnHCl prepared in 20 mM Tris-HCl buffer, pH 7.6. The concentration of the concentrated stock solution of GdnHCl was determined refractometrically (*35*). According to the method described by Muzammil et al. (*32*), in denaturation experiments, to a stock protein solution were added different volumes of the buffer first, and the denaturant was added last so as to get the desired concentration of denaturant. On the other hand, for renaturation experiments, to a stock protein solution were added different volumes of concentrated denaturant solution first, the mixture was incubated for 4 h, and finally buffer was added to get desired denaturant concentration. The final solution mixture for both the denaturation and renaturation experiment was incubated for 12 h at 25 °C before fluorescence measurements.

Refolding Kinetic Measurements. For the refolding kinetic measurements, 1 mL of the sample solution was continuously excited at 295 nm, and the emission intensity was collected at 340 nm for intrinsic fluorescence or at 545 nm for Tb^{3+} fluorescence with a response time of 2.0 s. The data were collected in the time scan mode after the refolding process was initiated by adding 2 μL of 0.5 M Ca^{2+} or 2 μL of 5 mM Tb^{3+} ions and continued for at least 40 min. The kinetic experiment was carried out three times to ensure that the results were reproducible.

Irreversible Thermal Denaturation. Apo-ACF II (1 μg/mL) and holo-ACF II (1 μg/mL) in 20 mM Tris-HCl buffer (pH 7.6) were incubated in the absence and presence of 1 mM $CaCl_2$, respectively, at the desired temperature for 30 min, followed by quenching in ice for 5 min, and finally, the anticoagulant activity of the protein was measured using a modification of the plasma prothrombin time (PPT) assay as described previously (*1*).

Data Analysis. Unfolding and refolding curves were analyzed using either two-state or three-state mechanisms.

Two-State Mechanism. The two-state model is represented as

$$\mathrm{N} \leftrightarrow \mathrm{D} \tag{1}$$

where N and D are the native and denatured states, respectively. The equilibrium constant is defined as

$$K = [\mathrm{D}]/[\mathrm{N}] \tag{2}$$

The fraction of each species is

$$f_\mathrm{N} = 1/(1 + K); \qquad f_\mathrm{D} = K/(1 + K) \tag{3}$$

The difference in free energy between the native and the unfolded states, ΔG, was calculated by the equation:

$$\Delta G = -RT \ln K \tag{4}$$

where R is the gas constant and T is the absolute temperature.

Three-State Mechanism. The three-state model used in the global analysis is (*36*)

$$\mathrm{N} \leftrightarrow \mathrm{I} \leftrightarrow \mathrm{D} \tag{5}$$

where N, I, and D are the native, intermediate, and denatured states, respectively. The two equilibrium constants describing the system are defined as

$$K_\mathrm{NI} = [\mathrm{I}]/[\mathrm{N}]; \qquad K_\mathrm{ID} = [\mathrm{D}]/[\mathrm{I}] \tag{6}$$

The fraction of each species is

$$\begin{aligned} f_\mathrm{N} &= 1/(1 + K_\mathrm{NI} + K_\mathrm{NI}K_\mathrm{ID}) \\ f_\mathrm{I} &= K_\mathrm{NI}/(1 + K_\mathrm{NI} + K_\mathrm{NI}K_\mathrm{ID}) \\ f_\mathrm{D} &= K_\mathrm{NI}K_\mathrm{ID}/(1 + K_\mathrm{NI} + K_\mathrm{NI}K_\mathrm{ID}) \end{aligned} \tag{7}$$

The free energy change corresponding to each equilibrium constant is

$$\Delta G_\mathrm{NI} = -RT \ln K_\mathrm{NI}; \qquad \Delta G_\mathrm{ID} = -RT \ln K_\mathrm{ID} \tag{8}$$

The measured signal, Y, is assumed to contain contributions from each species. For the two-state model

$$Y = f_\mathrm{N}Y_\mathrm{N} + f_\mathrm{D}Y_\mathrm{D} \tag{9}$$

For the three-state model

$$Y = f_\mathrm{N}Y_\mathrm{N} + f_\mathrm{I}Y_\mathrm{I} + f_\mathrm{D}Y_\mathrm{D} \tag{10}$$

where f_j represents the fraction of species j (as defined in eq 3 and eq 7) and Y_j is the molar signal of species j. The signals corresponding to the native and the unfolded state are considered as local fitting parameters that have a linear dependence on denaturant:

$$Y_\mathrm{j} = Y_\mathrm{j}^0 + \alpha_\mathrm{j}[\mathrm{GdnHCl}] \tag{11}$$

where Y_j^0 is the molar signal of species j at zero denaturant and α_j is a "slope" describing the dependence of signal Y_j on denaturant concentration. In the denaturant range where the unfolding process does not make a significant contribution to changes in the spectroscopic, eq 11 describes the "baseline" of species j. The signal of the intermediate, Y_I, is described by the nondimensional parameter Z (*36*)

$$Y_\mathrm{I} = (1 - Z)Y_\mathrm{N} + ZY_\mathrm{D} \tag{12}$$

where Z is considered to be a global fitting parameter.

ΔG corresponding to each equilibrium constant is assumed to be linearly dependent on [GdnHCl] denoted here by C, essentially as described in detail previously (*37*):

$$\Delta G = \Delta G^0 - mC = m(C_\mathrm{m} - C) \tag{13}$$

in which ΔG^0 and ΔG represent the free energy of unfolding or refolding in the absence and presence of GdnHCl, respectively, C_m is the midpoint concentration of GdnHCl required for unfolding or refolding, and m stands for the slope of the unfolding or refolding curve at C_m and is a measure of the dependence of ΔG on denaturant concentration.

The thermodynamic and spectroscopic parameters were optimized in global fits by nonlinear least-squares analysis using the Marquardt−Levenburg algorithm in a routine of software.

RESULTS

Steady-State Fluorescence of Tryptophan. The intrinsic fluorescence of Trp residues in ACF II was used for studies of its unfolding/refolding behavior. As there are 14 Trps in ACF II (*1*), the overall changes in fluorescence reflect global changes in protein structure, and average microenvironments of Trps can be assessed. The inset figure in Figure 2 shows

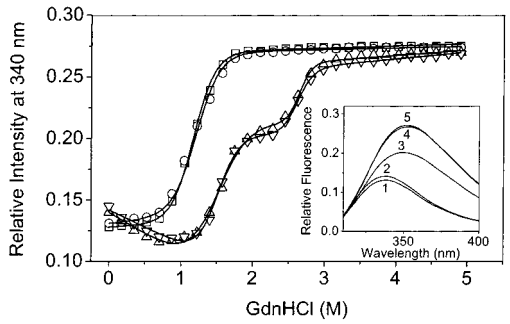

FIGURE 2: GdnHCl-induced unfolding and refolding of ACF II in 0.02 M Tris-HCl buffer, pH 7.6, 25 °C. The protein concentration of 1 μM was used in the study. Unfolding (□) and refolding (○) transitions of apo-ACF II and unfolding (△) and refolding (▽) transitions of holo-ACF II were monitored by measurement of fluorescence at 340 nm after excitation at 295 nm. The curves are the fitting curves based on experimental points by nonlinear least-squares analysis for the two-state transition of apo-ACF II according to eq 9 and by the global analysis for the three-state transition of holo-ACF II according to eq 10. The inset figure depicts the intrinsic fluorescence spectra of apo-ACF I in native (1) and 2.1 M GdnHCl unfolded (5) states and holo-ACF I in native (2), 2.1 M GdnHCl intermediate (3), and 4.9 M GdnHCl unfolded (4) states.

fluorescence emission spectra of apo-ACF II and holo-ACF II in native, 2.1 M GdnHCl, and 4.9 M GdnHCl unfolded states by exciting the protein at 295 nm. It is notable that the GdnHCl-induced unfolding causes the fluorescence emission intensities of both apo-ACF II and holo-ACF II to increase with the red shift of emission maximum λ_{max}, suggesting that both native apo-ACF II and holo-ACF II assume a compactly folded structure in which most Trps and quenchers, such as the charged carboxyl and/or amino groups in the interior protein, are adjacent as observed for bovine β-lactoglobulin (*38*). As shown in Figure 2, GdnHCl-induced denaturation of apo-ACF II was found to be a single-step process with no detectable intermediate state(s). The transition starts at around 0.65 M GdnHCl and slopes off at 1.85 M GdnHCl with a red shift of the λ_{max} (from 339 to 354 nm). The refolding transition curve of apo-ACF II essentially superposes on its unfolding transition curve, which shows the GdnHCl-induced denaturation of apo-ACF II is reversible. Ca^{2+} ions (1 mM) were present during holo-ACF II unfolding/refolding, since the occupation of the both Ca^{2+}-binding sites requires a concentration of Ca^{2+} ions of 1 mM (*2*). GdnHCl-induced denaturation of holo-ACF II was found to be a two-step process with accumulation of an intermediate state in a different manner to apo-ACF II. A Similar transition curve was obtained for the refolding of holo-ACF II, suggesting that GdnHCl-induced denaturation of holo-ACF II is also reversible. GdnHCl-induced denaturation of holo-ACF II is approximated to a three-state transition, and the mechanism for unfolding/refolding of holo-ACF II is represented as eq 5. The slight linear decrease of fluorescence intensity of holo-ACF II with no obvious λ_{max} shift at low concentrations of GdnHCl, less than 0.80 M, was observed, which was assumed the solvent perturbation effect on its fluorescence and therefore was regarded as a baseline. The first transition of holo-ACF II unfolding which corresponded to the transformation of the N state to the I state starts at around 1.10 M GdnHCl and completes at 1.95 M GdnHCl concentration with the increase of fluorescence intensity and a significant red shift of the λ_{max} from 339 to 350 nm, which indicates that the unfolding I state of holo-ACF II has extensively disordered structure. The I state is stable in the GdnHCl concentration range 1.95−2.20 M. The second transition, which corresponded to the unfolding of I state, starts at around 2.25 M GdnHCl and finally slopes off to the D state at 3.30 M GdnHCl concentration with a further increase of fluorescence intensity and a further red shift of the λ_{max} from 350 to 354 nm, suggesting that a few folding conformations probably exist in the I state which contains some local hydrophobic regions around some Trps.

The transitions of GdnHCl-induced unfolding and refolding of apo-ACF II in absence of Ca^{2+} follow a two-state mechanism, while GdnHCl-induced denaturation of holo-ACF II follows a three-state mechanism. The thermodynamic and spectroscopic parameters were obtained by nonlinear least-squares analysis for the two-state transition of apo-ACF II according to eq 9 and by the global analysis for the three-state transition of holo-ACF II according to eq 10. The ΔG^0, C_m, and m values obtained for the GdnHCl-induced unfolding transition of apo-ACF II are 4.60 ± 0.08 kcal mol^{-1}, 1.17 ± 0.04 M, and 3.92 ± 0.06 kcal M^{-1} mol^{-1}, respectively. The ΔG_{NI}^0, C_m^{NI}, and m_{NI} values obtained for the first transition (N ↔ I) of holo-ACF II are 4.99 ± 0.10 kcal mol^{-1}, 1.59 ± 0.03 M, and 3.14 ± 0.11 kcal M^{-1} mol^{-1}, respectively. Value of ΔG_{NI}^0 represents the difference in free energy between the native and the intermediate states of holo-ACF II in the absence of GdnHCl. However, it is more difficult to accurately calculate ΔG_{ID}^0 of holo-ACF II because, below 2.1 M GdnHCl, the intermediate state is not stable and will change to the native state; as a result, the free energy of unfolding ΔG_{ID} should not linearly depend on [GdnHCl] below 2.1 M GdnHCl and using eq 13 will lead to a wrong value for ΔG_{ID}^0. According to the method of Muzammil et al. (*32*), the free energy change of holo-ACF II in the presence of 1 mM Ca^{2+} associated with the N ↔ I ↔ D transition can be calculated by summing the free energy change of the individual steps, i.e., ΔG_{NI}^0 and ΔG_{ID}*, since ΔG, as a thermodynamic parameter, does not depend on the path. Value of ΔG_{ID}* represents the value obtained from extrapolation of ΔG_{ID} values up to the starting of the process (I ↔ D), 2.1 M GdnHCl. The ΔG_{ID}*, C_m^{ID}, and m_{ID} values associated with the second transition (I ↔ D) of holo-ACF II are 1.38 ± 0.04 kcal mol^{-1}, 2.57 ± 0.09 M^{-1}, and 2.86 ± 0.08 kcal M^{-1} mol^{-1}, respectively. The ΔG_{total}^0 of holo-ACF II in the presence of 1 mM Ca^{2+}, i.e., the free energy change associated with the transformation of the N state to the I state and finally to the D state, was calculated to be 6.37 ± 0.13 kcal mol^{-1}. A comparison of the free energy changes of apo-ACF II and holo-ACF II during GdnHCl-induced unfolding clearly indicates that the ΔG_{total}^0 of holo-ACF II in the presence of 1 mM Ca^{2+} is greater than the ΔG^0 of apo-ACF II in the absence of Ca^{2+}, and the difference is found to be 1.77 ± 0.13 kcal mol^{-1}. These results demonstrate that Ca^{2+} ions in holo-ACF II markedly stabilize its conformation.

Similar results are obtained for equilibrium parameters of refolding transitions of apo-ACF II and holo-ACF II in GdnHCl solution compared to their unfolding transition. The ΔG^0, C_m, and m values obtained for the GdnHCl-induced refolding transition of apo-ACF II are 4.42 ± 0.07 kcal mol^{-1}, 1.21 ± 0.02 M, and 3.64 ± 0.05 kcal M^{-1} mol^{-1}, respectively. The ΔG_{NI}^0, C_m^{NI}, and m_{NI} values obtained for the first refolding transition (N ↔ I) of holo-ACF II are 5.12

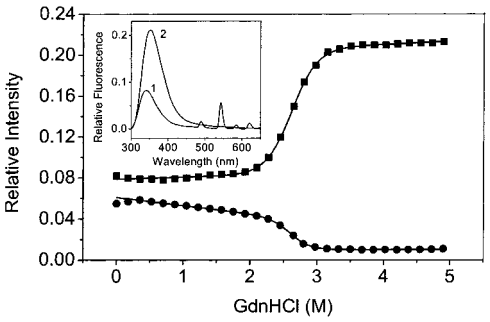

FIGURE 3: GdnHCl-induced unfolding of Tb^{3+}-reconstituted ACF II in 10 μM Tb^{3+} and 0.02 M Tris-HCl buffer, pH 7.6, 25 °C. The concentration of Tb^{3+}-ACF II is 1 μM. Unfolding transitions of Tb^{3+}-ACF II were monitored by measurement of Trp fluorescence at 340 nm (■) and Tb^{3+} fluorescence at 545 nm (●), respectively, after excitation at 295 nm. The curves are the fitting curves based on experimental points by nonlinear least-squares analysis according to eq 9. The inset figure shows the intrinsic fluorescence spectra of Tb^{3+}-ACF II in the native (1) and 4.9 M GdnHCl unfolded (2) states.

$\pm$ 0.13 kcal mol^{-1}, 1.50 $\pm$0.02 M, and 3.41 $\pm$ 0.08 kcal M^{-1} mol^{-1}, respectively, while the ΔG_{ID}*, C_m^{ID}, and m_{ID} values associated with the second refolding transition (I $\leftrightarrow$ D) of holo-ACF II are 1.41 $\pm$ 0.02 kcal mol^{-1}, 2.62 $\pm$ 0.03 M^{-1}, and 2.94 $\pm$ 0.08 kcal M^{-1} mol^{-1}, respectively. The difference of refolding free energy (N $\leftrightarrow$ D) for holo-ACF II in the presence of 1 mM Ca^{2+} and apo-ACF II in the absence of Ca^{2+} is 2.11 $\pm$ 0.15 kcal mol^{-1}. The result also suggests that Ca^{2+} ions increase the conformational stability of holo-ACF II to the similar extent as determined from its unfolding transition.

Tb^{3+} Steady-State Fluorescence. Tb^{3+} has higher affinity to ACF II than Ca^{2+} and can completely replace both Ca^{2+} in holo-ACF II. The apparent association constants of Tb^{3+} are (2.1 $\pm$ 0.2) $\times$ 10^7 M^{-1} and (1.0 $\pm$ 0.1) $\times$ 10^7 M^{-1} (*39*). The binding of Tb^{3+} to ACF II causes the intrinsic fluorescence of ACF II to decrease and results in the characteristic fluorescence emission of Tb^{3+} from its $^5D_4$ excited state to ^7F_j (j = 6, 5, 4, 3) state at 488, 545, 580, and 620 nm, respectively, by excitation at 295 nm (*39*). This characteristic emission of Tb^{3+} upon its binding to ACF II is due to the nonradiative energy transfer between Trps and the bound Tb^{3+} ions in ACF II (*40*). Considering that the structural changes of the Tb^{3+}-binding sites should affect the characteristic emission of Tb^{3+}, we measured the changes in emission intensity both at 340 nm and at 545 nm during equilibrium unfolding of Tb^{3+}-ACF II to determine whether Tb^{3+} could be used as a fluorescence probe to monitor the structural change of the Ca^{2+}-binding sites during unfolding/refolding.

Because occupation of both metal ion-binding sites of ACF II requires 10 μM Tb^{3+} and high concentration of Tb^{3+} will cause the precipitation of Tb^{3+} ions at pH 7.6, 10 μM Tb^{3+} was present during the unfolding of Tb^{3+}-ACF II. Figure 3 shows the GdnHCl-induced unfolding of Tb^{3+}-ACF II as monitored by the measurements of the intrinsic fluorescence at 340 nm and the Tb^{3+} fluorescence at 545 nm, respectively, by exciting the protein at 295 nm. The GdnHCl-induced unfolding of Tb^{3+}-ACF II induces an increase in the fluorescence intensity of Trps and decreases in the intensities of the four fluorescence peaks of Tb^{3+} at 488, 545, 580, and 620 nm (inset figure in Figure 3). GdnHCl-induced denaturation of Tb^{3+}-ACF II was found to be a single-step process with no detectable intermediate state(s) when studied by both intrinsic fluorescence and Tb^{3+} fluorescence. The transition monitored by the measurements of intrinsic fluorescence at 340 nm shows that the abrupt unfolding of Tb^{3+}-ACF II starts at around 2.06 M GdnHCl and completes at about 3.30 M GdnHCl with a red shift of the λ_{em} (340 $\rightarrow$ 352 nm), while the transition monitored by the measurements of Tb^{3+} fluorescence at 545 nm shows that the abrupt unfolding of Tb^{3+}-ACF II starts at around 2.09 M GdnHCl and completes at about 3.20 M GdnHCl. The midpoint of the red shift of the λ_{em} of Trps occurs at around 2.60 M GdnHCl, within experimental errors, which is very similar to the midpoint (2.65 M GdnHCl) for the change of the Tb^{3+} emission intensity. These results demonstrate that the unfolding of Tb^{3+}-ACF II leads to the disruption of both compact Tb^{3+}-binding regions at the same time and breaks the nonradiative energy transfer from Trp residues to both bound Tb^{3+} ions.

Using a two-state (N $\leftrightarrow$ D) mechanism, the ΔG^0, C_m, and m values for the GdnHCl-induced unfolding transition of Tb^{3+}-ACF II were obtained to be 7.26 $\pm$ 0.11 kcal mol^{-1}, 2.60 $\pm$ 0.03 M, and 2.79 $\pm$ 0.04 kcal M^{-1} mol^{-1} as monitored by the measurements of intrinsic fluorescence at 340 nm and 7.48 $\pm$ 0.20 kcal mol^{-1}, 2.65 $\pm$ 0.05 M, and 2.82 $\pm$ 0.12 kcal M^{-1} mol^{-1} as monitored by the measurements of Tb^{3+} fluorescence at 545 nm, respectively. A comparison of the free energy changes of Tb^{3+}-ACF II and holo-ACF II during GdnHCl-induced unfolding clearly indicates that the ΔG^0 of Tb^{3+}-ACF II is greater than the ΔG_{total}^0 of holo-ACF II, and the difference is found to be 0.89 $\pm$ 0.13 kcal mol^{-1} as monitored by the measurements of intrinsic fluorescence at 340 nm. The result suggests that Tb^{3+}-stabilized ACF II exhibits higher resistance to GdnHCl denaturation than holo-ACF II.

CD Measurements. To test if the unfolding transition monitored by fluorescence reflects a disruption of the overall structure of the protein or just a local unfolding, we analyzed the GdnHCl-induced denaturation of ACF II using far-UV CD spectroscopy. All native apo-ACF II, holo-ACF II, and Tb^{3+}-ACF II have a similar far-UV CD spectrum (data not shown). The α-helix and β-sheet contents of holo-ACF II have been estimated to 18.6% and 26.2%, respectively, using a method reported by Chen et al. (*41*). Similar results were obtained for apo-ACF II (17.8% for α-helix and 25.5% for β-sheet) and for Tb^{3+}-ACF II (19.1% for α-helix and 25.2% for β-sheet), which suggests that both Ca^{2+} and Tb^{3+} have no obvious effect on the secondary structure of ACF II. The secondary structure contents of habu IX/X-bp on the basis of the X-ray structure are 19.0% for α-helix, 24.6% for β-sheet, and 56.4% for other structures (*7*). Within experimental errors, the α-helix and β-sheet contents of holo-ACF II, apo-ACF II, and Tb^{3+} -ACF II are very similar to habu IX/X-bp, which further suggests that ACF II probably has a backbone structure similar to that of habu IX/X-bp.

The changes in ellipticity at 222 nm for the protein incubated in various concentrations of GdnHCl were used to construct the stability profiles. As shown in Figure 4, all transition profiles of apo-ACF II, holo-ACF II, and Tb^{3+} -ACF II show a single step with no apparent intermediate state(s). Using a two-state mechanism, the ΔG^0, C_m, and m values for the GdnHCl-induced unfolding transition of apo-ACF II, holo-ACF II, and Tb^{3+}-ACF II monitored by the

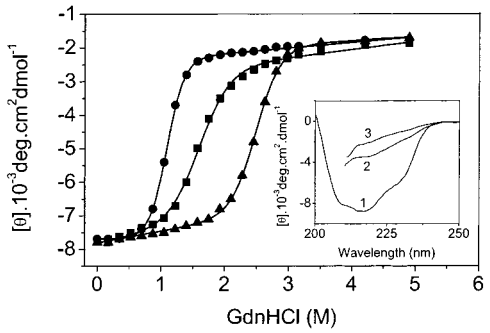

FIGURE 4: GdnHCl-induced changes of the far-UV CD spectra of ACF II in 0.02 M Tris-HCl buffer, pH 7.6, 25 °C. The protein concentration is 0.10 mg/mL. Changes in far-UV CD ellipticity at 222 nm of apo-ACF II (●), holo-ACF II (■), and Tb^{3+}-ACF II (▲). The curves are the fitting curves based on experimental points by nonlinear least-squares analysis according to eq 9. The inset figure shows the far-UV CD spectra of holo-ACF II in the native (1), 2.1 M GdnHCl intermediate (2), and 4.9 M GdnHCl unfolded (3) states.

measurements of ellipticity at 222 nm were calculated to be 4.65 ± 0.08, 4.97 ± 0.16, and 7.22 ± 0.12 kcal mol^{-1}, 1.12 ± 0.03, 1.60 ± 0.04, and 2.49 ± 0.05 M, and 4.16 ± 0.10, 3.11 ± 0.08, and 2.90 ± 0.05 kcal M^{-1} mol^{-1}, respectively.

The transition of apo-ACF II monitored by the measurements of ellipticity at 222 nm shows that the abrupt unfolding of apo-ACF II starts at around 0.66 M GdnHCl and completes at about 1.80 M GdnHCl. The ΔG^0 (4.65 ± 0.08 kcal mol^{-1}) estimated from the far-UV ellipticity is similar to that based on fluorescence spectroscopy (4.60 ± 0.08 kcal mol^{-1}). The normalized transition curves for GdnHCl-induced unfolding of apo-ACF II monitored by the measurements of ellipticity at 222 nm and fluorescence at 340 nm are nearly superimposable (data not shown). These results further suggest that the GdnHCl-induced unfolding process of apo-ACF II follows a two-state (N ↔ D) mechanism without the accumulation of stable equilibrium intermediate(s).

The transition of holo-ACF II monitored by the measurements of ellipticity at 222 nm shows that the abrupt unfolding of holo-ACF II starts at around 1.04 M GdnHCl and completes at about 2.78 M GdnHCl (Figure 4). The normalized transition curve for GdnHCl-induced unfolding of holo-ACF II monitored by the measurements of ellipticity at 222 nm and the normalized transition curve for the GdnHCl-induced first transition (N ↔ I) of holo-ACF II monitored by the fluorescence at 340 nm are nearly superimposable (data not shown), suggesting that the two-state transition of holo-ACF II monitored by the measurements of ellipticity at 222 nm corresponds to the first transition (N ↔ I) of holo-ACF II monitored by the fluorescence at 340 nm. The unfolding ΔG^0 (4.97 ± 0.16 kcal mol^{-1}) estimated from the far-UV ellipticity is similar to $\Delta G_{NI}{}^0$ of the N ↔ I transition of holo-ACF II based on fluorescence spectroscopy (4.99 ± 0.10 kcal mol^{-1}). However, the existence of the second unfolding transitions monitored by the fluorescence measurements, i.e., I ↔ D, was not detected by far-UV CD measurements. These results further demonstrate that the unfolding I state of holo-ACF II is extensive disordering of the native structures only with retaining a few secondary structures.

The transition of Tb^{3+}-ACF II monitored by the measurements of ellipticity at 222 nm shows that the abrupt unfolding of Tb^{3+}-ACF II starts at around 1.74 M GdnHCl and completes at about 3.20 M GdnHCl (Figure 4). The normalized transition curves for GdnHCl-induced unfolding of Tb^{3+}-ACF II monitored by the measurements of ellipticity at 222 nm and fluorescence at 340 nm or at 545 nm are nearly superimposable (data not shown). These results further indicate that the GdnHCl-induced unfolding process of Tb^{3+}-ACF II is single step without the accumulation of detectable equilibrium intermediate(s). The ΔG^0 (7.22 ± 0.12 kcal mol^{-1}) estimated from the far-UV ellipticity during GdnHCl-induced unfolding is similar to that based on fluorescence spectroscopy (7.26 ± 0.11 and 7.48 ± 0.20 kcal mol^{-1} monitored by the measurements of fluorescence at 340 and 545 nm, respectively) and is also greater than the $\Delta G_{total}{}^0$ of holo-ACF II based on fluorescence spectroscopy (6.37 ± 0.13 kcal mol^{-1}). These results further prove that Tb^{3+}-stabilized ACF II exhibits higher resistance to GdnHCl denaturation than the holo-ACF II.

Metal Ion-Induced Refolding of ACF II. Because Ca^{2+} and Tb^{3+} ions can increase the structural stability of ACF II, higher concentrations of denaturant are required to induce it to unfold for holo-ACF II and Tb^{3+}-ACF II than for apo-ACF II. It is possible to find a denaturant concentration at which refolding from the fully denatured state to the intermediate state or to the native state could be initiated by adding the metal ion to the unfolded state. It is obvious from Figures 2 and 3 that, at 2.1 M GdnHCl, apo-ACF II is in the denatured state, while holo-ACF II and Tb^{3+}-ACF II are in the I state and the native state, respectively. Therefore, it might be possible to perform a refolding jump from the unfolded state of apo-ACF II to the I state of holo-ACF II by adding the Ca^{2+} ions or from the unfolded state of apo-ACF II to the native state of Tb^{3+}-ACF II by adding the Tb^{3+} ions to the unfolded state of apo-ACF II. Such transitions could be monitored by fluorescence measurements. It was found that, without adding metal ions, unfolded apo-ACF II exhibited no change in intrinsic fluorescence spectrum after 1 h at 2.1 M GdnHCl concentration. The intrinsic fluorescence intensity of apo-ACF II began to decrease after addition of 1 mM Ca^{2+} to the unfolded apo-ACF II, and the fluorescence intensity of Tb^{3+} began to increase with the decrease of the intrinsic fluorescence intensity of apo-ACF II after addition of 10 μM Tb^{3+} to the unfolded apo-ACF II. The quenching of Trp fluorescence by Ca^{2+} and Tb^{3+} and the enhancing of Tb^{3+} reflect the formation of compact metal-binding regions, suggesting metal ion-induced refolding of the protein. There were no further changes of the fluorescence spectra observed after 40 min of refolding, indicating that the refolding process was completed within this time.

The refolding kinetics was monitored by Trp fluorescence at 340 nm and by Tb^{3+} fluorescence at 545 nm after addition of metal ions to the unfolded apoprotein. Figure 5 shows the representative kinetic traces. The kinetics of Ca^{2+}-induced refolding monitored by Trp fluorescence at 340 nm could not be satisfactorily fit to a single-exponential function. A sum of two-exponential terms best fits the refolding curve yielding refolding rate constant values of 0.0890 ± 0.0009 and 0.0091 ± 0.0002 s^{-1} for the faster and slower phases, respectively. The kinetics of Tb^{3+}-induced refolding was also

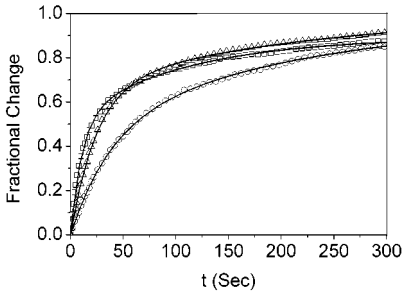

FIGURE 5: Metal ion-induced refolding of apo-ACF II from the unfolded state in 2.1 M GdnHCl and 0.02 M Tris-HCl buffer, pH 7.6, monitored by measurement of fluorescence by excitation at 295 nm. Refolding was initiated by addition of 1 mM Ca^{2+} (□, quenching of Trp fluorescence at 340 nm) or 10 μM Tb^{3+} (○, quenching of Trp fluorescence at 340 nm; △, enhancing of Tb^{3+} fluorescence at 545 nm) to 1 μM apo-ACF II in 2.1 M GdnHCl. All curves were obtained after fitting to a sum of two-exponential terms based on experimental points.

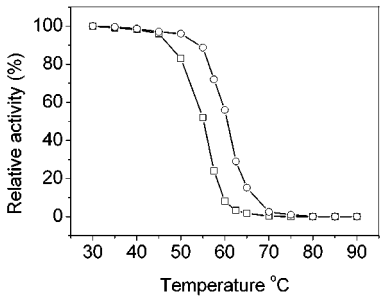

FIGURE 6: Irreversible thermal denaturation of apo-ACF II and holo-ACF II in 0.02 M Tris-HCl buffer, pH 7.6. The irreversible thermal unfolding transitions of apo-ACF II (□) in the absence of Ca^{2+} and holo-ACF II (○) in the presence of 1 mM Ca^{2+} were determined by monitoring the loss in their anticoagulant activity associated with the increase in temperature. The protein concentration was 1.0 μg/mL. Data are expressed in terms of relative activity using the activity of native holo-ACF II as reference (100%).

best fitted to a sum of two-exponential terms yielding refolding rate constant values of 0.0262 ± 0.0005 and 0.0046 ± 0.0002 s^{-1} for the faster and slower phases, monitored by Trp fluorescence at 340 nm, and rate constant values of 0.0408 ± 0.0006 and 0.0044 ± 0.0001 s^{-1} for the faster and slower phases, monitored by Tb^{3+} fluorescence at 545 nm, respectively.

Irreversible Thermal Denaturation. Irreversible thermal denaturation studies on apo-ACF II and holo-ACF II have been conducted by incubating the protein at variable temperatures for 30 min and evaluating the denaturation of the protein by monitoring the loss in their anticoagulant activity associated with the increase in temperature. Figure 6 shows the effect of increasing the temperature on the loss of the anticoagulant activity in the temperature range of 30−90 °C. For both apo-ACF II and holo-ACF II, a sigmoidal decrease in activity with increasing temperature was observed. However, a difference in the temperature corresponding to irreversible thermal denaturation of the protein under these conditions was observed between apo-ACF II and holo-ACF II. Figure 6 clearly shows that the decalcification of holo-ACF II results in about a 5 °C left shift of the irreversible thermal denaturation curve, which indicates that Ca^{2+}-stabilized holo-ACF II exhibits higher resistance against thermal denaturation than apo-ACF II.

DISCUSSION

One of the most intriguing observations in the present study is that Ca^{2+} ions not only increase the structural stability of ACF II but also influence its unfolding/refolding behavior. The GdnHCl-induced unfolding/refolding of apo-ACF II in the absence of Ca^{2+} is a two-state process with no detectable intermediate(s), while the GdnHCl-induced unfolding/refolding of holo-ACF II in the presence of 1 mM Ca^{2+} follows the three-state transition with an intermediate state. As shown in Figure 2, the decalcification of holo-ACF II shifts both the initial and ending zones of the unfolding/refolding curve toward lower GdnHCl concentrations and abolishes the formation of intermediate in the absence of Ca^{2+} ions. It can be deduce from these results that Ca^{2+} ions should play an important role in the stabilization of the structures of the native and I states. The I state should be unstable at higher GdnHCl concentration in the absence of Ca^{2+} ions; as a result, the GdnHCl-induced unfolding/refolding of apo-ACF II in the absence of Ca^{2+} is a two-state process with no intermediate.

As shown in Figure 2, the two transition curves for the unfolding and refolding of holo-ACF II in the presence of 1 mM Ca^{2+} are almost superimposable, which suggests that the intermediate state should be an on-pathway intermediate. On the basis of this assumption, the goodness of the fit of a three-state equilibrium model (N ↔ I ↔ D) by the global analysis for refolding of holo-ACF II further demonstrates that the intermediate state is on-pathway for refolding of holo-ACF II.

The different unfolding/refolding transition curves for holo-ACF II and apo-ACF II suggest that the intermediate of holo-ACF II should still have calcium bound. Addition of 1 mM Ca^{2+} to the unfolded apo-ACF II causes the intrinsic fluorescence intensity of apo-ACF II to decrease (Figure 5), while unfolded apo-ACF II exhibits no change in intrinsic fluorescence spectrum after addition of 5 mM Na^{+} to the unfolded apo-ACF II (unpublished data), which reveals that Ca^{2+}-induced fluorescence quenching of unfolded apo-ACF II is not due to the change of the ionic strength of the solution. Because Ca^{2+} ions have no direct quenching (such as collisional quenching and energy transfer quenching) effect on the fluorescence of tryptophan (unpublished data), Ca^{2+}-induced fluorescence quenching of unfolded apo-ACF II should be attributed to the complex formation between protein and Ca^{2+}, and this binding then induces the formation of the intermediate and perturbs the microenvironment around the relevant tryptophan residue(s) and therefore causes the fluorescence quenching of protein. This result further indicates that the intermediate of holo-ACF II still has calcium bound. However, we cannot infer whether the intermediate has one or two calciums bound from the present data. Further investigation is necessary to clarify this issue.

The I state of holo-ACF II at 2.10 M GdnHCl seems to have the following characteristics: (i) the loss of native structure, according to the significant increase of intrinsic fluorescence intensity from the N state to the I state; (ii) the loss of most secondary structure as indicated by marked change of far-UV CD spectra from the N state to the I state; (iii) the retention of a few folding conformations within local hydrophobic regions, as judged from the fact that the second transition from the I state to the D state of holo-ACF II results

in a further increase of fluorescence intensity by 30% with a red shift of the λ_{max} from 350 to 354 nm and a further decrease of ellipticity at 222 nm by 21%; (iv) the exposure of the most Trp residues, based on the significant red shift of the intrinsic fluorescence from the N state to the I state; (v) the retention of calcium bound.

It is obvious from Figures 2 and 3 that the GdnHCl concentrations required for the complete unfolding of holo-ACF II and Tb^{3+}-ACF II are almost identical, but the binding of Tb^{3+} ions to ACF II shifts the initial zone of the denaturation curve toward higher GdnHCl concentration, thus abolishing the formation of intermediate in the presence of 10 μM Tb^{3+} ions. In other words, Tb^{3+} ions have stronger ionic potentials and are able to more strongly stabilize the native conformation of ACF II than Ca^{2+} ions, which can be inferred from the greater free energy change ΔG^0 of Tb^{3+}-ACF II than the $\Delta G_{total}{}^0$ of holo-ACF II. Therefore, a higher concentration of GdnHCl is required to induce the protein unfolding, at which the I state should be unstable; as a result, Tb^{3+}-ACF II has undergone a single-step transition with no detectable intermediate in the presence of 10 μM Tb^{3+} ions.

Interestingly enough, by comparing the denaturation profiles of apo-ACF II, holo-ACF II, and Tb^{3+}-ACF II, we found that, under appropriate denaturing condition (2.1 M GdnHCl), a refolding jump could be initiated. Indeed, we were able to initiate refolding of unfolded apo-ACF II simply by adding 1 mM Ca^{2+} or 10 μM Tb^{3+}. Fluorescence measurements show that both refolding processes from the unfolded state of apo-ACF II to the I state of holo-ACF II induced by 1 mM Ca^{2+} and from the unfolded state of apo-ACF II to the native state of Tb^{3+}-ACF II induced by 10 μM Tb^{3+} are best fit to a sum of two-exponential terms, suggesting a faster and a slower folding population in both processes (Figure 5). It is interesting to note that similar refolding rate constant values of the slower phase (0.0046 ± 0.0002 and 0.0044 ± 0.0001 s^{-1}) for the process of Tb^{3+}-induced refolding were obtained by measurements of Trp fluorescence at 340 nm and Tb^{3+} fluorescence at 545 nm, but the refolding rate constant values of the faster phase (0.0262 ± 0.0005 and 0.0408 ± 0.0006 s^{-1}) were very different as monitored by Trp fluorescence at 340 nm and Tb^{3+} fluorescence at 545 nm. Tb^{3+} fluorescence measurements can detect the first and the last phases, while Trp fluorescence measurements can detect the second and the last phases. The fastest refolding rate associated with the first phase was obtained from Tb^{3+} fluorescence measurements, indicating that Tb^{3+} ions are rapidly bound to the protein initially and the fastest step should involve the formation of the compact metal-binding site regions. Subsequently, the protein undergoes further conformational rearrangements, which correspond to the second step and the last step to form its native structure as observed from the further decrease of the intrinsic fluorescence and the further increase of Tb^{3+} fluorescence. Although we cannot infer the detailed picture of the pathway of the metal ion-induced refolding from the present data, it is certain that the metal ion-induced refolding of apo-ACF II could be performed without changing the concentration of the denaturant. Further investigation is necessary to elucidate the structure of the intermediate state and the mechanism of the metal ion-induced refolding.

Protein activity can be regarded as the most sensitive probe for studying the changes in the protein conformation during denaturation as it reflects subtle readjustments at the active site. However, it is very difficult to trace the change of the anticoagulant activity of ACF II during its unfolding and refolding. Anticoagulant activity was determined using a modification of the plasma prothrombin time (PPT) assay as described previously (*1*). When we measured the anticoagulant activity of ACF II during its unfolding and refolding, we found that GdnHCl had a marked effect on its PPT. Even though, in the absence of ACF II rabbit plasma did not clot in 0.30 M GdnHCl after 12 h incubation of the plasma with thromboplastin and 5 mM Ca^{2+}. A plausible explanation is that GdnHCl is a competitive inhibitor of the trypsin-like serine proteases in the coagulation cascade. It is also difficult to trace the change of the binding ability of ACF II to FXa in the denaturation process for a possible reason that FXa, as a protein, may be also affected by GdnHCl. After extensive dialysis of 6.0 M GdnHCl-denatured holo-ACF II against 0.02 M Tris-HCl buffer (pH 7.6) containing 1 mM Ca^{2+} to remove GdnHCl, it almost recovered the full anticoagulant activity in the native state, suggesting that GdnHCl-induced denaturation of holo-ACF II is reversible.

It has been reported that habu IX/X-bp undergoes a conformational change upon binding of Ca^{2+} ions and forms a crystal only when 3 mM Ca^{2+} ions are present, indicating that it adopts a loose, amorphous conformation and a rigid, ordered conformation in the absence and presence of Ca^{2+} ions, respectively (*42*). Similarly, holo-ACF II exhibits much higher resistance to GdnHCl denaturation than the apo-ACF II, indicating it should have a significantly more compact conformation than the apoprotein. The stabilizing effect of Ca^{2+} ions on the overall structure of holo-ACF II was also confirmed by studying the irreversible thermal denaturation of apo-ACF II and holo-ACF II. From these results, we speculate that Ca^{2+} ions may play similar roles in keeping protein structure and function for ACF II as well as for habu IX/X-bp.

It has been reported that the two Ca^{2+} ions in habu IX/X-bp can be all replaced by trivalent lanthanide ions such as Lu^{3+} and Sm^{3+} (*7*). The sites of Lu^{3+} and Sm^{3+} in heavy-atom soaked crystals of habu IX-bp are identical with that of Ca^{2+} (*8*). Similarly, trivalent lanthanide ions, such as Nd^{3+}, Sm^{3+}, Eu^{3+}, Gd^{3+}, and Tb^{3+}, can completely substitute the Ca^{2+} ions in holo-ACF II. The binding of Tb^{3+} ions to ACF II has been analyzed by equilibrium dialysis, and two Tb^{3+}-binding sites are identified in the presence of 10 μM Tb^{3+} (*39*). Tb^{3+}, as a trivalent ion, has stronger ionic potential and therefore has stronger stabilization of the conformation of ACF II than holo-ACF II, as inferred from the higher initial zone of the denaturation curve of Tb^{3+}-ACF II than that of holo-ACF II. However, the binding of ACF II with FXa is dependent on Ca^{2+} ions, while trivalent lanthanide ions, such as Nd^{3+}, Sm^{3+}, Eu^{3+}, Gd^{3+}, and Tb^{3+}, are all ineffective to induce the binding (unpublished work). The particular GdnHCl-induced transition profile of holo-ACF II, compared to that of apo-ACF II and Tb^{3+}-ACF II, reveals that Ca^{2+} ions play unique roles in stabilizing the specific conformation of holo-ACF II. The Ca^{2+} ion-stabilized specific conformation of holo-ACF II should be helpful to its recognition of the structure of FXa, thereby promoting the association of two proteins. However, trivalent lanthanide

ions have stronger ionic potentials in contrast with Ca^{2+} ions; thus, the Tb^{3+} ion-stabilized conformation of Tb^{3+}-ACF II may be unsuitable for its recognition of the conformation of FXa and cannot support the binding of Tb^{3+}-ACF II with FXa. Another possible reason for the dependence of the binding of ACF II with FXa on Ca^{2+} ions may be that FXa itself is a Ca^{2+}-binding protein with multiple Ca^{2+}-binding sites and the binding of Ca^{2+} ions to FXa also induces the conformational changes of FXa (*43*−*47*). Thus, the binding of Ca^{2+} ions to ACF II and FXa not only induces the conformational change of ACF II but also induces the conformational change of FXa, and both conformational changes might be essential for the recognition of each other.

CONCLUSIONS

Metal ions not only increase the structural stability of ACF II against GdnHCl denaturation and irreversible thermal denaturation but also influence its unfolding/refolding behavior. The GdnHCl-induced unfolding/refolding of apo-ACF II and Tb^{3+}-ACF II is a single-step process with no detectable intermediate state, while the GdnHCl-induced unfolding/refolding of holo-ACF II in the presence of 1 mM Ca^{2+} follows the two-step transition with an intermediate state. Ca^{2+} ions play an important role in the stabilization of both native and I states of holo-ACF II. Tb^{3+}-stabilized ACF II exhibits higher resistance to GdnHCl denaturation than the holo-ACF II. It is possible to induce refolding of the unfolded apo-ACF II merely by adding 1 mM Ca^{2+} ions or 10 μM Tb^{3+} ions without changing the concentration of the denaturant. The kinetic results of metal ion-induced refolding provide evidence for the fact that the first phase of Tb^{3+}-induced refolding should involve the formation of the compact metal-binding site regions, and subsequently, the protein undergoes further conformational rearrangements to form the native structure.

ACKNOWLEDGMENT

We thank Dr. Hongyu Hu for assistance with the CD measurements. We also thank Dr. Zhongliang Zhu for help in preparation of the manuscript.

REFERENCES

1. Xu, X. L., Liu, Q. L., Xie, Y. S., and Wu, S. D. (2000) *Toxicon 38*, 1517−1528.
2. Xu, X. L., and Liu, Q. L. (2001) *Toxicon 39*, 1359−1365.
3. Sekiya, F., Atoda, H., and Morita, T. (1993) *Biochemistry 32*, 6892−6897.
4. Atoda, H., Ishikawa, M., Yoshihara, E., Sekiya, F., and Morita, T. (1995) *J. Biochem. 118*, 965−973.
5. Chen, Y. L., and Tsai, I. H. (1996) *Biochemistry 35*, 5264−5271.
6. Atoda, H., Ishikawa, M., Mizuno, H., and Morita, T. (1998) *Biochemistry 37*, 17361−17370.
7. Mizuno, H., Fujimoto, Z., Koizumi, M., Kano, H., Atoda, H., and Morita, T. (1997) *Nat. Struct. Biol. 4*, 438−441.
8. Mizuno, H., Fujimoto, Z., Koizumi, M., Kano, H., Atoda, H., and Morita, T. (1999) *J. Mol. Biol. 289*, 103−112.
9. Dobson, C. M., and Karplus, M. (1999) *Curr. Opin. Struct. Biol. 9*, 92−101.
10. Englander, S. W. (2000) *Annu. Rev. Biophys. Biomol. Struct. 29*, 213−238.
11. Samuel, D., Kumar, T. K. S., Balamurugan, K., Lin, W. Y., Chin, D. H., and Yu, C. (2001) *J. Biol. Chem. 276*, 4134−4141.
12. Valente-Mesquita, V. L., Botelho, M. M., and Ferreira, S. T. (1998) *Biophys. J. 75*, 471−476.
13. Sasahara, K., Sakurai, M., and Nitta, K. (2001) *Proteins: Struct., Funct., Genet. 44*, 180−187.
14. Chapeaurouge, A., Johansson, J. S., and Ferreira, S. T. (2001) *J. Biol. Chem. 276*, 14861−14866.
15. Scalley, M. L., and Baker, D. (1997) *Proc. Natl. Acad. Sci. U.S.A. 94*, 10636−10640.
16. Griko, Y. V., and Remeta, D. P. (1999) *Protein Sci. 8*, 554−561.
17. Benitez-Cardoza, C. G., Rojo-Dominguez, A., and Hernandez-Arana, A. (2001) *Biochemistry 40*, 9049−9058.
18. Perez, J., Vachette, P., Russo, D., Desmadril, M., and Durand, D. (2001) *J. Mol. Biol. 308*, 721−743.
19. Bedell, J. L., McCrary, B. S., Edmondson, S. P., and Shriver, J. W. (2000) *Protein Sci. 9*, 1878−1888.
20. Jamin, M., and Baldwin, R. L. (1998) *J. Mol. Biol. 276*, 491−504.
21. Whitten, S. T., Wooll, J. O., Razeghifard, R., Garcia-Moreno, B., and Hilser, V. J. (2001) *J. Mol. Biol. 309*, 1165−1175.
22. Gupta, S., Warne, A., Saraste, M., and Mazumdar, S. (2001) *Biochemistry 40*, 6180−6189.
23. Cheng, H., Sukal, S., Callender, R., and Leyh, T. S. (2001) *J. Biol. Chem. 276*, 9931−9935.
24. Liu, X. Q., and Wang, C. C. (2001) *J. Biol. Chem. 276*, 1146−1151.
25. Sedlak, E., Valusova, E., Nesper-Brock, M., Antalik, M., and Sprinzl, M. (2001) *Biochemistry 40*, 9579−9586.
26. Chaudhuri, A. R., Khan, I. A., and Luduena, R. F. (2001) *Biochemistry 40*, 8834−8841.
27. Ahmad, A., Akhtar, M. S., and Bhakuni, V. (2001) *Biochemistry 40*, 1945−1955.
28. Yuan, C., Xie, Z. Q., Zhang, F. W., and Xu, G. J. (2001) *J. Protein Chem. 20*, 39−47.
29. Alexander, P. A., Ruan, B., and Bryan, P. N. (2001) *Biochemistry 40*, 10634−10639.
30. Deswarte, J., De Vos, S., Langhorst, U., Steyaert, J., and Loris, R. (2001) *Eur. J. Biochem. 268*, 3993−4000.
31. Apiyo, D., Jones, K., Guidry, J., and Wittung-Stafshede, P. (2001) *Biochemistry 40*, 4940−4948.
32. Muzammil, S., Kumar, Y., and Tayyab, S. (2000) *Proteins Struct., Funct., Genet. 40*, 29−38.
33. Edwin, F., and Jagannadham, M. V. (2000) *Arch. Biochem. Biophys. 381*, 99−110.
34. Andersson, D., Hammarstrom, P., and Carlsson, U. (2001) *Biochemistry 40*, 2653−2661.
35. Nozaki, Y. (1972) *Methods Enzymol. 26*, 43−50.
36. Ionescu, R. M., Smith, V. F., O'Neill, J. C., and Matthews, C. R. (2000) *Biochemistry 39*, 9540−9550.
37. Pace, C. N. (1990) *Trends Biotechnol. 8*, 93−98.
38. Sakai, K., Sakurai, K., Sakai, M., Hoshino, M., and Goto, Y. (2000) *Protein Sci. 9*, 1719−1729.
39. Xu, X. L., Liu, Q. L., and Xie, Y. S. (2001) *Chem. J. Chin. Univ. 22*, 1807−1812.
40. Dong, W. J., Robinson, J. M., Xing, J., Umeda, P. K., and Cheung, H. C. (2000) *Protein Sci. 9*, 280−289.
41. Chen, Y. H., Yang, J. T., and Chau, K. H. (1974) *Biochemistry 13*, 3350−3359.
42. Mizuno, H., Atoda, H., and Morita, T. (1991) *J. Mol. Biol. 220*, 225−226.
43. Jackson, C. M. (1984) *Prog. Hemostasis Thromb. 7*, 55−109.
44. Sunnerhagen, M., Forsen, S., Hoffren, A. M., Drakenberg, T., Teleman, O., and Stenflo, J. (1995) *Nat. Struct. Biol. 2*, 504−509.
45. Stenflo, J. (1991) *Blood 78*, 1637−1651.
46. Sunnerhagen, M., Drakenberg, T., Forsen, S., and Stenflo, J. (1996) *Haemostasis 26*, 45−53.
47. Sunnerhagen, M., Olah, G. A., Stenflo, J., Forsen, S., Drakenberg, T., and Trewhella, J. (1996) *Biochemistry 35*, 11547−11559.

BI015819J